FINAL REPORT
U. S. Department of Energy

HIGH FREQUENCY ELECTROMAGNETIC IMPEDANCE IMAGING FOR VADOSE ZONE AND GROUNDWATER CHARACTERIZATION

Principal Investigator:
Gregory A. Newman
Sandia National Laboratories

Collaborators:
David L. Alumbaugh
University of Wisconsin Madison

Michael Hoversten
Lawrence Berkeley National Laboratory

Edward Nichols
ElectroMagnetic Instruments Inc.
Richmond CA.

Project Number: DE-FG07-99ER15021
Project Period: 9/15/1999 - 9/14/2002

Table of Contents

1 Executive Summary 2
2 Research Objectives 2
3 Methods and Results 4
3.1 The Hanford Reservation Test Site 4
3.2 The Electromagnetic Impedance Method 6
3.3 The 3D Electromagnetic Impedance Inversion Algorithm 8
3.4 3D Analysis and Inversion of Hanford Impedance Data 10
3.5 Conclusions 14
4 Relevance, Impact and Technology Transfer 15
5 Project Productivity 15
6 Personnel Supported 15
7 Publications 15
8 Future Work 15
9 Literature Cited 16
10 Feedback 17
11 Figures 18

List of Figures

Figure 1. Map of the Hanford Nuclear Reservation located in central Washington State (from Linsey et al., 1999). 18
Figure 2. Structure of clastic injection dikes encountered at the Hanford Nuclear Reservation 18
Figure 3. STRATAGEM Impedance System employed at the Hanford Nuclear Reservation. Roving receiver station is composed of electric dipoles (Ex0, Ex1, Ey0 and Ey1), magnetic sensors (Hy and Hx), and a analog front end (taken from the EMI website). 19
Figure 4. Detailed site map 19
Figure 5. Shown are the transmitter and receiver geometry employed at the Hanford Nuclear Reservation field site. Also shown is the inverted conductivity model at the earth's surface, z=0 m, where the clastic dike structures are indicated in red with a black out 20
Figure 6. Surface plot of combined impedance data $||(Zxy+Zyx)||$ at 66 kHz over the clastic dike site (Army Loop Road Site in Figure 4). The dikes indicated by the yellow to red shading are clearly seen in the plot, and clearly exhibit three-dimensional geometry. 20
Figure 7. Surface plot of impedance data, Zxy and Zyx, respectively. These data were taken at 66 kHz over the clastic dike site. The dikes indicated by the yellow to red shading are clearly seen in the plot, and clearly exhibit three-dimensional geometry. 21
Figure 8. Observed and Predicted Zxy data plotted as apparent resistivity pseudo sections along four profiles in the y coordinate direction. 22
Figure 9. Observed and Predicted Zyx data plotted as apparent resistivity pseudo sections along four profiles in the y coordinate direction. 23
Figure 10. Depth sections of the reconstructed electrical conductivity of the Hanford field data. 24
Figure 11. Three-dimensional model used to study the resolving power of near field CSAMT data. Multiple receivers transect the dike, identical to the survey configuration used in the Hanford experiment, but only three of these receiver transects are shown at the 25
Figure 12. Reconstructed conductivity depth sections for the 3D test model. 26
Figure 13. Three-dimensional radio magnetotelluric image of a waste site in Cologne Germany. Resistivities greater than 50 W.m have been rendered invisible, except along selected cross sections. The volumetric extent of the waste is confined to within the top 15 27

1 Executive Summary

A geophysical experiment is described for characterizing the clastic dike systems, which are ubiquitous within the vadose zone at the Hanford Nuclear Reservation. Because the dikes possess a significant electrical contrast from the insulating host medium, we have applied controlled source audio magnetotelluric (CSAMT) measurements to map their geometric extent and to further clarify if the dike complex acts as a conduit for contaminant transport within the vadose zone. Because of cost and weak natural field signal levels, we employed controlled field sourcing using the STRATGEM acquisition system. Use of artificial fields often comes with the assumption that the data are acquired in the far-field of the transmitter. Hence the data can be interpreted using standard plane wave processing algorithms. Because field data were acquired essentially in the mid to near field, due to instrument limitations, we have developed a 3D inversion scheme that includes the source effects, and can properly treat data acquired in the near to mid field. Unfortunately our findings show that the CSAMT data acquired in the near to mid field lack sufficient resolving power to map the clastic dike complex at the Hanford test site below 10 m depth. Hence the resolving power of the method appears to be inadequate for studying, at a sufficient level detail, the dike complex, and its ability to act as a conduit for contaminant transport within the vadose zone. In order to achieve the desired model resolution at increased depth, use of a more powerful source for acquiring far-field data would be beneficial. Another alternative would be to use a variant of the MT method that utilizes far-field radio transmitters. This method possesses significant potential for characterizing near-surface geology, relevant to hydrological investigations, and overcomes the limitations using weak natural field signals.

2 Research Objectives

At many United States Department of Energy (DOE) facilities, the presence of toxic or radioactive waste within the subsurface poses a serious and ongoing threat to public health and safety. The contamination has resulted from free releases of waste on the surface, from leaking landfills and/or leaking tanks, or any number of other scenarios. In addition many leaks have occurred

above the water table. I.e. within the vadose zone, which is often dominated by heterogeneous deposits that are geologically chaotic in nature. Thus transport and flow within the vadose zone is a complex process that in many cases is not well understood, and often contaminants have shown up where they were not expected. In addition, predictive groundwater modeling is often based on the assumptions of a fairly uniform and homogenous unsaturated zone, which grossly underestimates the spread of contamination. A specific example of a possible catastrophe caused by a poor understanding of contaminant transport was discovered at the Hanford Reservation, several years ago, where it was determined that subsurface waste was on the verge of seeping into the Columbia River, in a location previously thought to be contaminant free.

Therefore, accurate descriptions of transport pathways on the gross scale, the location of contamination, and characterization of heterogeneity within the vadose zone, are now realized as vital for proper treatment, confinement and stabilization of subsurface contamination at DOE waste sites. Electromagnetic (EM) methods are ideal for these tasks since they are directly sensitive to the amount of fluid present in porous media, as well as fluid composition. At many DOE sites it is necessary to employ low frequency (<1 MHz) or diffusive electromagnetic fields because of the inability of ground penetrating radar (GPR) to penetrate to sufficient depths. The high frequency electromagnetic impedance method, which operates in the diffusive frequency range (10 Hz to 1 MHz), is an ideal technique to delineate and map the aforementioned targets. The method has clearly shown the potential to provide needed information on variations in subsurface saturation due to leaking storage tanks and perched water zones, as well as mapping geological structures related to the subsurface hydrological properties and heterogeneity within the vadose zone. In consideration of this technique, higher frequencies provide greater resolution, but are limited in their penetration depths. To achieve greater depths require measurements at lower frequencies. However such measurements come at the expense of reduced resolution. Resolution can be roughly quantified using the concept of a skin depth. Assuming an average or bulk earth resistivity, ρ, and frequency, f, at a measurement site, the skin depth, which measures the effective penetration of the electromagnetic field, is given by $\delta = 503\sqrt{\rho / f}$. As a rule of thumb, our ability to resolve features in the earth are on the order of

¼ δ for impedance methods, provided the measurements are made at sufficient distance from the sources of the EM fields.

Although it exhibits certain advantages over other EM methods, the impedance method comes with a set of assumptions and practices that can limit its potential. The first is the desire to locate receivers in the far field of the transmitter, which allows the use of magnetotelluric inversion codes to interpret the data. Unfortunately, one does not precisely know when one is in the far field of the transmitter, because it depends upon the geology we desire to image. The second limiting factor is the scarcity of complete 3D inversion schemes necessary to properly invert the data; 2D and layered imaged schemes already exist but are limited in characterizing complex 3D transport pathways within the vadose zone. While approximate 3D schemes are available for interpreting the data, their range of applicability is poorly known, adding more uncertainty to the data interpretation process. Thus rigorous 3D inversion codes are needed to provide bounds on the applicability of the approximate methods. We have attempted to address the above mentioned problems in the following manner: (1) implemented a full non-linear 3D inversion scheme that incorporates source coordinates and polarization characteristics to relax the constraint that data be acquired in the far field of the transmitter, (2) used the scheme to study the impact on image resolution when data are acquired in the mid and near field of the transmitter, (3) collected several data sets at the Hanford Reservation and (4) interpreted the field data using the newly developed 3D inversion capability.

3 Methods and Results

3.1 The Hanford Reservation Test Site

The Hanford Nuclear Reservation occupies 560 square miles of land in the Pasco Basin of central Washington State. The area is bordered to the north and east by the Columbia River and to the south by the Rattlesnake Mountains (Figure 1). The location of the facility was largely based upon the remote location of the Pasco Basin and its close proximity to the Columbia River, which provided the water necessary to cool the nuclear reactors used to generate plutonium .It has been extensively studied due to the ongoing production of plutonium and other site activities carried out up until the

late 1970's. At present, many types of chemically complicated and high-level nuclear wastes are resting in more than 100 underground storage tanks scattered throughout the Reservation (Hall, 2000a). Although all plutonium production has ceased, the site is now the focal point of a massive clean up effort headed by the US Department of Energy. As of the year 2000, 66 of the underground storage tanks were known to be leaking and, due to the large amount of hazardous wastes produced, over 400 billion gallons of liquid wastes have been directly disposed in soils distributed throughout the Reservation (Hall, 2000b). It is the DOE's mission to locate and treat all of the contaminated areas within the site and keep the waste from entering the Columbia River and local groundwater (Department of Energy Home page, 2001).

The extent of the leaking of waste at the Hanford Reservation may lie in the presence of clastic injection dikes scattered throughout the Pasco basin. These dikes are associated with multiple ages of emplacement, including at least 3 different periods of the Pleistocene epoch (Lindsey et al., 1999). They are embedded within glacial-fluvial sediment suggesting that the formation took place during or soon after large glacial-fluvial flooding events. These dikes formed as a result of buoyant rise of low density, water rich mud, into the overlying glacial-fluvial sediment. Individual dikes seem to have formed during a continuous, but relatively short, process; including the formation of fissures and gradual widening of fissure apertures, and infilling of clastic sediments. The overall structure of the dykes consists of a silty clay outer shell with infilling of fine sands that form a seeming impermeable barrier (Figure 2). These dikes are ubiquitous in the vadose zone at the Hanford Site, and may act as a pathway for contaminant transport as fluids are wicked along the dike surfaces. Thus the answer to stabilizing and thereby containing the leaking waste at Hanford, may lie in first mapping the extent and location of the clastic injection dikes.

Composed of fine-grained material, mostly fine sand, silt and clay, the dikes are estimated to have an average electrical resistivity of 60 Ω-m while the background glacial-fluvial sediment ranges from 600 to 250 Ω-m. At the surface the dikes range from 0.5 to 2 meters in width and in some cases stretch over 100 meters in length. Of major importance is the vertical and lateral extent of the dikes and detecting the existence of the original horizontal mud layer from which the dikes originated. If this layer is large enough to produce the dikes and still be horizontally continuous throughout the site, the

dike network may act as a bowl, impeding any liquid wastes from entering into the local groundwater supply. However, if this layer is not present the vertical dikes may act as transport pathways, quickly wicking away liquid wastes from leaking storage tanks into the groundwater supply.

3.2 The Electromagnetic Impedance Method

The magnetotelluric (MT) and audio magnetotelluric (AMT) methods are frequency domain electromagnetic (EM) sounding techniques, which employ naturally occurring magnetic (H) and electric (E) fields to investigate the three-dimensional conductivity structure of the earth. The origin of these EM fields is located far from the measuring site. Because of the high conductivity of the earth, the wave propagates as a plane wave, in a direction perpendicularly incident to the earth's surface.

The MT method makes use of naturally occurring EM energy in the frequency range of 0.0005 Hz to 100 Hz, which is generated by the flow of charged particles in the earth's ionosphere and their interaction with the earth's internally produced magnetic field (Vozoff, 1972). AMT utilizes EM energy generated by distant thunderstorms, which cause electric and magnetic field disturbances in the frequency range of 100 Hz to 10 kHz (Zonge and Hughes, 1991). In both cases, the electric and magnetic fields are measured at the Earth's surface using orthogonal electric dipoles and magnetic coils (Sharma, 1997). By casting the measured field quantities in terms of impedance, which is basically a ratio of electric to magnetic field, the source characteristics of the measured field are removed, greatly simplifying the data interpretation process.

The controlled source audio magnetotelluric (CSAMT) method is an extension of the above mentioned natural field methods and operates in the frequency range from 100 Hz to 10 MHz. The method employs a transmitter to produce artificial fields to replace the use of weak natural fields, speeding up data acquisition time, in the field and reducing errors due to cultural noise. Depending upon the source receiver separation, resistivity of the subsurface, and the frequency being employed, conventional plane wave analysis can be used to interpret the data. On the other hand, if the receiver is located is in the near field (less than 3 skin depths from the transmitter) the data will be saturated with source effects, resulting in uncharacteristic apparent resistivity and phase readings when analyzed using conventional MT inversion (Goldstein and Strangway, 1975; Unsworth et al., 2000; and Sandberg and Hohmann, 1982). In order to obtain accurate inversion results with near field CSAMT

data, the inversion/imaging algorithm must account for the three-dimensional nature of the source fields produced at the transmitter.

The natural fields employed in the MT and AMT methods have an infinite number of polarizations. Hence all elements of the impedance tensor can be estimated from a minimal amount of measurements of Ex, Ey, Hx and Hy (Ward and Hohmann, 1988). Artificial signals in contrast, have one finite location and polarization, which require the employment of two independent, orthogonal source polarizations in order to compute the impedance tensor at the measurement site; when the earth is not one-dimensional, the impedance measurement, must be described as a tensor

$$Z = \begin{bmatrix} Z_{xx} Z_{xy} \\ Z_{yx} Z_{yy} \end{bmatrix} \tag{1}$$

where Z is the impedance tensor, which relates the measured magnetic field to the electric field at a given measurement site and frequency

$$\begin{bmatrix} E_x \\ E_y \end{bmatrix} = \begin{bmatrix} Z_{xx} Z_{xy} \\ Z_{yx} Z_{yy} \end{bmatrix} \begin{bmatrix} H_x \\ H_y \end{bmatrix}. \tag{2}$$

When two orthogonal source polarizations are used to determine the impedance tensor at a specific frequency, its elements are specified with the following formulas found in Newman and Alumabugh, 2000:

$$Z_{xx} = \frac{E_{x1}H_{y2} - E_{x2}H_{y1}}{H_{x1}H_{y2} - H_{x2}H_{y1}} \tag{3}$$

$$Z_{xy} = \frac{E_{x2}H_{x1} - E_{x1}H_{x2}}{H_{x1}H_{y2} - H_{x2}H_{y1}} \tag{4}$$

$$Z_{yx} = \frac{E_{y1}H_{y2} - E_{y2}H_{y1}}{H_{x1}H_{y2} - H_{x2}H_{y1}} \tag{5}$$

$$Z_{yy} = \frac{E_{y2}H_{x1} - E_{y1}H_{x2}}{H_{x1}H_{y2} - H_{x2}H_{y1}}. \tag{6}$$

The plane wave aspects of the CSAMT technique have been thoroughly examined by Goldstein and Strangway (1975), Sandberg and Hohmann (1982), Zonge and Hughes (1991) and others. It has been shown that CSAMT data collected in the far field regime can be properly interpreted using conventional MT or plane wave techniques. According to Sandberg and Hohmann (1982) and Goldstein and Strangway (1975), the transmitter must be at least 3 skin depths from the measurement site to satisfy the far field conditions. Depending on field conditions, Zonge and Huges (1991) use a minimum transmitter-receiver separation of 4 skin depths. Sandberg and Hohmann (1982) show that CSAMT apparent resistivity data collected in the far field are within 10% of the plane wave apparent resistivites. Nevertheless, due to transmitter power limitations, it is not always possible to produce measurable source signals in the far field. Thus CSAMT/impedance measurements are often made in the near field, where the nature of the source fields emitted from the transmitter are 3D and the incident EM wave is not orthogonal to the surface of the earth. In other words the plane wave assumption no longer applies. In order to interpret such data in a self-consistent manner requires that the source location and polarizations be taken into account, in the presence of a 3D earth model. This will be accomplished using a 3D inversion framework described next.

3.3 The 3D Electromagnetic Impedance Inversion Algorithm

Below, we give a cursory description of the 3D MT inversion algorithm to be used in the analysis of the Hanford test site data. The difference in this algorithm from that described in the paper of Newman and Alumbaugh (2000) is that the plane wave assumption is relaxed. The impedance elements are computed by first specifying two orthogonal magnetic dipole source polarizations, at a fixed location and frequency. Other than this critical difference, the 3D EM impedance inversion scheme follows closely the description given in Newman and Alumbaugh, 2000. Following that paper

we divide the 3D earth into M prismatic cells and assign to each cell an unknown conductivity value. Let **m** be a vector of length M that describes these values. The regularized least squares cost functional to be minimized in the inversion process, which combines the data error and model smoothness constraint will be given by

$$\varphi = \{\varepsilon^{-1}(\mathbf{Z}^{obs}-\mathbf{Z}^{pre})\}^{H}\{\varepsilon^{-1}(\mathbf{Z}^{obs}-\mathbf{Z}^{pre})\} + \lambda\, \mathbf{m}^{T}\mathbf{W}^{T}\mathbf{W}\mathbf{m} \qquad (7)$$

where H denotes the Hermitian operator. In equation (1), $\mathbf{Z}^{obs}$ and $\mathbf{Z}^{pre}$ are data vectors that represent the predicted and observed magnetotelluric impedances at different frequencies and locations. These are complex values, and a given entry in the data vector can represent any component of the impedance tensor given in equation (1). ε^{-1} in equation (7) is a diagonal matrix that contains the inverse of the data error estimates. Here noisier data are given smaller weight, or less importance, when forming φ, than good quality data.

The regularization parameters that stabilize the inverse problem (Tikhonov and Arsenin, 1977) enforce a model smoothness constraint. While other constraints are available, we have selected to employ this constraint because it is easy to implement and yields stable solutions that can map spatially varying geological media reasonably well. In equation (7) the regularization parameters are given by the matrix **W**, which consists of a finite difference approximation to the Laplacian (∇^2) operator, and the trade-off parameter λ. This later parameter is used to control the amount of smoothness to be incorporated into the model. In its selection, we note that a large parameter will produce a highly smooth model, but this model will show poor dependence on the data. A small parameter, on the other hand, will give a superior data fit, but the resulting model may be too rough and non-physical. Following Newman and Alumbaugh (2000), equation (7) is in principle minimized multiple times with different tradeoff parameters that are fixed, and the smoothest model that provides an acceptable match to the data within observational errors is selected as the optimal result.

To insure that the inverted conductivity is positive, a lower bounding constraint has been implemented in the minimization of equation (7). This constraint allows the user to designate the

lowest conductivity value that the model can attain on a cell-by-cell basis. This constraint is actually implemented by inverting for the logarithm of the parameters (cf., Newman et al., 2002; Newman and Alumbaugh, 2000). Because of the size of the 3D inverse problem, gradient methods are the only practical methods for the minimization of equation (7). The method of steepest descent is the easiest and simplest to implement of the gradient methods. Unfortunately it usually converges very slowly in practice. A better approach is the method of nonlinear conjugate gradients (NLCG), first proposed by Fletcher and Reeves (1964) for nonlinear optimization, and later improved by Polyak and Ribière (1969) and recently implemented in 2D and 3D MT inversion algorithms (cf., Rodi and Mackie, 2001; Newman and Alumbaugh, 2000). The method is closely related to the linear CG method of Hestenes and Stiefel (1952) and is in fact identical if the cost functional is quadratic. We refer interested readers to the above references, where more information on the NLCG method can be found with specific details required for the MT data inversion, including efficient evaluation of the cost functional, its gradient, and practical line search procedures required by this minimization method.

3.4 3D Analysis and Inversion of Hanford Impedance Data

The impedance data collected at the Hanford Nuclear Reervation were obtained using the "STRATAGEM" electrical conductivity imaging system, from EMI (Electromagnetic Instruments Inc., Berkeley, California); Figure 3. The field setup consisted of two-fixed orthogonal loop magnetic transmitters, a roving receiver, acquisition console, AFE (analog front end) and two batteries. The magnetic transmitters operate over a frequency range from 1 to 70 kHz and possess a magnetic dipole moment of about 400 A-m^2 (Geometrics Home Page, 2001). The survey was conducted in 2000 at the "Army Loop Road" site (Figure 4). During October 22 through November 2, 2001 an additional survey was also completed at the Hanford Reservation at a different field site. Data analysis from this second survey is not reported here.

Impedance data were acquired at 231 locations on the surface of the earth for eleven frequencies ranging from 1.12 to 66.2 kHz (see Table 1 for a list of all of the frequencies employed) and provided estimates of the apparent resistivity and phase characteristics of the subsurface. The roving receiver station consisted of two three-meter orthogonal electric dipoles and two orthogonal magnetic sensing coils, just under one-meter in length. The receiver grid was constructed of eleven receiver

transects, each containing twenty-one stations, spaced three meters apart, yielding a grid size of 30 by 60 meters, with a receiver spacing of 3 meters in each direction, as illustrated in Figure 5.

Table 1. Plane wave skin depths calculated for the frequencies ( ) employed at the Hanford Nuclear Reservation using a average resistivity (=600 W.m) from the field site.

Frequency	Resistivity	Skin Depth	3 Skin Depths
Hz	Ohm-m	Meters	meters
1120	600	368	1104
1850	600	286	858
2540	600	245	735
3560	600	206	618
5060	600	173	519
6620	600	151	453
11200	600	116	348
15000	600	101	303
30500	600	71	213
51200	600	54	162
66200	600	48	144

Table 1 lists the plane wave skin depth for each of the frequencies employed at the Hanford Nuclear Reservation, using an average resistivity of 600 Ω.m to represent the background resistivity of the glaciofluvial host. The values in the last column of the table indicate the distance at which each frequency is considered to be in the far field, which for this analysis is assumed to be three times the skin depth (Sandberg and Hohamnn, 1982, and Goldstein and Strangway, 1975). Note that even at the highest frequencies all of the receiver stations in Figure 5 for Line 1, and most of the stations Lines 5 and 8, lie in the near field and will therefore contain non-plane wave effects imparted by the transmitter. Attempts were made to locate the transmitters further out from the survey area, but due to poor signal to noise characteristics it was not possible to acquire useable data.

As a first cut at interpreting the data, we have plotted the sum of the impedance $||Z_{xy}+Z_{yx}||$ at 66 kHz in Figure 6. This surface plot clearly indicates the spatial 3D geometry of the clastic dike complex. To better understand the sensitivity of the impedance measurements to the dike structures, we have plotted in Figure 7 apparent resistivity surface maps for the two source polarizations that give rise to Z_{xy} and Z_{yx} impedance data at 66 kHz. Apparent resistivity is a simple mathematical transform applied to the impedance data (Z_{xy} or Z_{yx}) at a specific location and frequency. Assuming the data are acquired

in the far field, this transform provides a resistivity estimate of a corresponding half-space. It is quite useful for making a quick assessment of the subsurface electrical properties, but does not provide any depth information. Nevertheless, it is clear from Figure 7, that the different parts of the dike structures are illuminated from the two independent source polarizations. In the case of the Z_{xy} polarization, dike structure striking along the y-direction is observed, while in the Z_{yx} polarization, we observe dike structure striking along the x-direction. Therefore to properly image the dike structure requires treatment of both source polarizations. Moreover, because the surface expression of the dike complex is clearly 3D in character, detailed analysis of the data should involve 3D modeling and inversion. This is necessary to provide a better understanding of the dike-complex subsurface geometry.

Using the 3D inversion scheme described earlier, which incorporates source effects, we have simultaneously inverted the impedance data for both Z_{xy} and Z_{yx} source polarizations. Figures 8 and 9 show the observed and predicted data, plotted as apparent resistivity pseudo sections, over the 66 kHz to 10k Hz frequency band. Good correspondence is seen between the observed and predicted data, with superior data fits nearer the transmitters. The 3D character in the data is clearly seen in Figure 8 and 9, where the change in dike geometry is clearly indicated in the plots; compare the observed and predicted data profiles at y=0 m to other profiles at y=12, 21 and 30 m. The data also show that statics are present in the Z_{xy} source polarization, centered near x=30 m along all profiles (Figure 8), but far less so in the Z_{yx} polarization. The statics are observed by the "*pull up*" in the apparent resistivity over the dike structure. Statics are caused by a boundary polarization charge induced when the electric field is polarized perpendicular to dike's geological structure. Because a significant component of the dike complex strikes along the y direction the statics would tend to be more pronounced for Z_{xy} polarization. The lack of statics in the Z_{yx} polarization, further implies that data interpretation assuming a 2D transverse electric (TE) field sourcing may be sufficient, provided that selected data profiles cross dike structure that exhibits approximate 2D geometry. For example, inspection of Figure 5, indicates that data analyzed along the line 8 profile could qualify. Persichetti (2002) attempted such a 2D analysis of the Hanford data, but achieved marginal success because the data were assumed to have been acquired within the far field. As we have mentioned previously, and

indicated in Table 1, the Hanford data are strongly influenced by near-field source effects and these effects must be considered in the data inversion/interpretation process.

The 3D reconstructed conductivity model obtained from the inversion of the Hanford data is shown in Figures 5 and 10. Figure 5, provides the clearest map of the dike complex, at the earth surface; dike structures are indicated in red with a black outline. However with increasing depth, we observe a rapid loss in model resolution. Loss in resolution is so great that it is not possible to make any definitive assessment on the geometry of the dike complex beyond 13 m depth. It is also worthwhile to point out that the conductivity estimates of the dikes, where they are well resolved, appear to be low. Site measurements indicate the resistivity of the dikes to be near 60 Ω.m or in terms of conductivity, 0.0167 S/m. However the inversion yields conductivity estimates of the dike complex at the earth's surface (Figure 5) to be about three times too small. Despite this poor estimate, the reconstructions clearly can map the geometric extent of the dikes in the near surface.

At this point two critical questions arise. Is the loss in model resolution due to acquiring and analyzing data in the near field, and/or due to the deficiencies in the accuracy of the 3D inversion scheme? While the 3D imaging scheme incorporates source geometry within the inversion process, and can treat data ranging from the near to the far field, it may not possess enough accuracy to image near-field data. On the other hand, near-field data may not possess sufficient information for mapping the dike complex beyond 13 m depth; Table I, clearly shows that with decreasing frequency, the data acquisition is progressively more within the near field and, more than likely, near field data are primarily sensitive to source geometry and far less too the subsurface geology. In contrast, the sensitivity of far field data is just the opposite. Since the dike complex is imaged quite well in the near surface, we suspect that the loss in model resolution with depth is due to a loss in the resolving power of the data.

To test the accuracy of the 3D imaging code, we considered a synthetic test model of the dike complex in Figure 11, where the transmitter was located at x=-40 m, y=15m as in Figure 5. At this separation, the only the data acquired at the highest frequency can considered far field for the longer receiver offsets, at other offsets and frequencies the data can still be characterized as mid to near field. Five percent random noise was added to the simulated data and then inverted using a 600 Ω.m

half space as a starting model; note the data were generated using the same finite difference code embedded within the 3D inversion code, necessary for computing the cost functional, predicted data, and gradients. After forty two inversion iterations, acceptable data fits were achieved, where the data component of the cost functional (the first term in equation 7) decreased from an initial value of 101.5 to 2.25, approaching a target misfit of one. In principle, a misfit value of one implies we have fit the data to within the estimated noise, assuming that the noise is Gaussian and normally distributed. Nevertheless inversion results for this test example (Figure 12) still shows a significant loss in model resolution below 10 m depth, and it was not possible to map the deeper structure of the dike complex. This result indicates that in order to get sufficient sensitivity of the deeper dike structures may require significantly larger transmitter-receiver offsets, necessary to insure all field measurements over the 60 kHz to 10 kHz frequency band are in the far field. Such offsets are considered not feasible given the noise limitations on STRATGEM acquisition system.

3.5 Conclusions

It appears that the CSAMT data acquired in the near to mid field lacks sufficient resolving power to map the clastic dike systems at the Hanford test site, below 10 m depth. Thus the resolving power of the method must be improved before it can be used to study at a sufficient level detail the dike systems, and hopefully help in accessing whether the clastic dikes act as a conduit for contaminant transport within the vadose zone. In order to achieve the desired model resolution at increased depth, use of a more powerful source for acquiring far-field data would be beneficial. Another alternative would be to use a variant of the MT method that utilizes far-field radio transmitters (Newman et al., 2003). This method shows significant potential for characterizing near surface geology, relevant to hydrological investigations. Figure 13 shows a 3D conductivity image of a waste site, near Cologne Germany, based upon the method. Because the data used in this example, which spans the frequency band, 200 kHz to 20 kHz, has been acquired in the far field, they possess sufficient resolving power to map the waste.

4 Relevance, Impact and Technology Transfer

This project attempted to map potential pathways for contamination transport within the vadose zone at the Hanford Reservation. Hence it addressed a waste legacy issue of critical interest to the United States Department of Energy. Unfortunately the project's impact was marginalized because the field data did not possess sufficient resolving power to map the dike complex below 10 m depth.

5 Project Productivity

Project productivity was good.

6 Personnel Supported

Mike Hoversten, Staff Member, Earth Science Division, Lawrence Berkeley National Laboratory

Joseph Persichetti, Master Student, Department of Geological Engineering, University of Wisconsin-Madison

7 Publications

Newman, G. A., Recher, S., Tezkan, B. and Neubauer, F., 2003, Three-dimensional inversion of a scalar radio magnetotelluric field data set: Geophysics in press.

Persichetti, J., 2002, Interpretation of 3-D controlled source audio magnetotelluric data collected at the Hanford Nuclear Reservation using 2-D inversion algorithms: Master Thesis, University of Wisconsin, Madison.

Newman, G. A., Hoversten, G. M., Alumbaugh, D. L., and Nichols, E., High frequency electromagnetic impedance imaging for vadose zone and groundwater characterization: EMSP Final Report, Project Number EMSP-70220.

8 Future Work

None planned

9 Literature Cited

Department of Energy (DOE) Hanford Site Home Page, 24 Oct. 2001: US Department of Energy, http://www.hanford.gov

Fletcher, R. and Reeves, C. M., 1964, Function minimization by conjugate gradients: Comp. J., **7**, 149-154. Geometrics Home Page, 12 Nov. 2001: http://www.geometrics.com/index.html

Goldstein, M. A. and Strangway, D. W., 1975, Audio-frequency magnetotellurics with a grounded electric dipole source: Geophysics, **40**, 669-683.

Hall, J., 2001a, "History of Hanford site defense production. Part I: 11 Oct. 2000, http://www.hanford.gov/history/misc/defn-1st.htm

Hall, J., 2001b, "History of Hanford site defense production. Part 2: 11 Oct. 2000, http://www.hanford.gov/history/misc/defn-2nd.htm

Hestenes, M. R. and Stiefel, E., 1952, Methods of conjugate gradients for solving linear systems, J. Res. Nat. Bureau, **49**, 409-436.

Lindsey, K. A., Bjornstadt, B. N., Horton, D. G., Fecht, K. R., Last, G. V., and Riedel, S. P., 1999, Clastic injection dikes of the Pasco Basin vicinity, *Bechtel Hanford Inc.*

Newman, G. A., Recher, S., Tezkan, B. and Neubauer, F., 2003, Three-dimensional inversion of a scalar radio magnetotelluric field data set: Geophysics in press.

Newman, G. A., Hoversten, G. M. and Alumbaugh, D. L., 2002, Three-dimensional magnetotelluric modeling and inversion: In Three-Dimensional Electromagnetics, Proceedings of the Second International Symposium, 127-152, Elsevier.

Newman, G. A., and Alumbaugh, D. L., 2000, Three-dimensional magnetotelluric inversion using non-linear conjugate gradients: Geophys. J. Int. **140**, 410-424.

Persichetti, J., 2002, Interpretation of 3-D controlled source audio magnetotelluric data collected at the Hanford Nuclear Reservation using 2-D inversion algorithms: Master Thesis, University of Wisconsin, Madison.

Polyak, E. and Ribière, G., 1969, Note sur la convergence des mèthods conjugèes: Rev. Fr. Inr. Rech. Oper., **16**, 35-43.

Rodi, W. and Mackie, R. L., 2001, Non linear conjugate gradients algorithm for 2D magnetotelluric inversion: Geophysics, **66**, 174-187.

Sandberg, S. K., and Hohmann, G. W.,1982, Controlled-source audiomagnetotellurics in geothermal exploration, Geophysics, **47**, 110-116.

Sharma, P. V., 1997, Environmental and Engineering Geophysics, United Kingdom: *The Press Syndicate of the University of Cambridge.*

Tikhonov, A. N. and Arsenin, V. Y., 1977, Solutions to ill posed problems: Wiley, New York, NY.

Unsworth, M. J., Lu, X., and Watts, M. D., 2000, CSAMT exploration at Sellafield: Characterization of a potential radioactive waste disposal site, Geophysics, **65**, 1070-1079.

Vozoff, K., 1972, The magnetotelluric method on the exploration of sedimentary basins, Geophysics, **37**, 98-141.

Ward, S. H., and Hohmann, G. W., 1988, Electromagnetic theory for geophysical applications, in Nabighian, M. N., Ed., Electromagnetic methods – Theory and practice, Society of Exploration Geophysics, **1**, 131-311.

Zonge K. L., and Hughes, L. J., 1991, Controlled source audio-frequency magnetotellurics: in Nabighain., M. N., Ed., Electromagnetic methods in applied geophysics, Society of Exploration Geophysics, **2**, 713-809.

10 Feedback

None

11 Figures

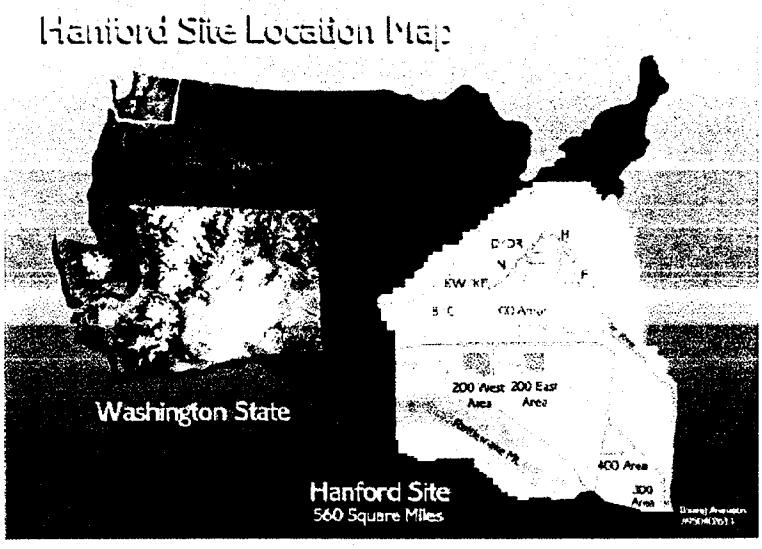

Figure 1. Map of the Hanford Nuclear Reservation located in central Washington State (from Linsey et al., 1999).

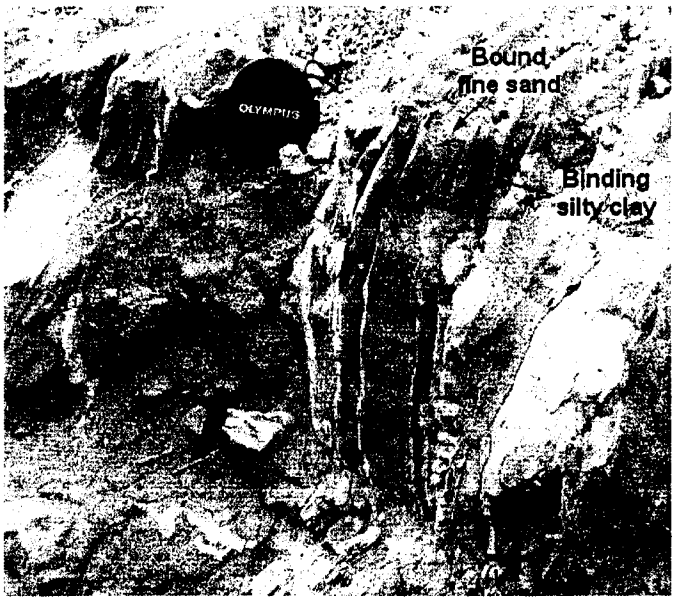

Figure 2. Structure of clastic injection dikes encountered at the Hanford Nuclear Reservation

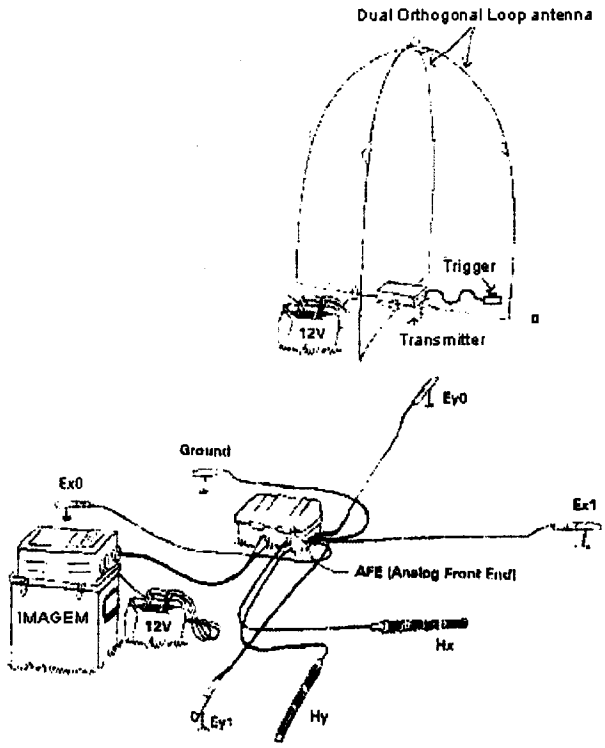

Figure 3. STRATAGEM Impedance System employed at the Hanford Nuclear Reservation. Roving receiver station is composed of electric dipoles (Ex0, Ex1, Ey0 and Ey1), magnetic sensors (Hy and Hx), and a analog front end (taken from the EMI website).

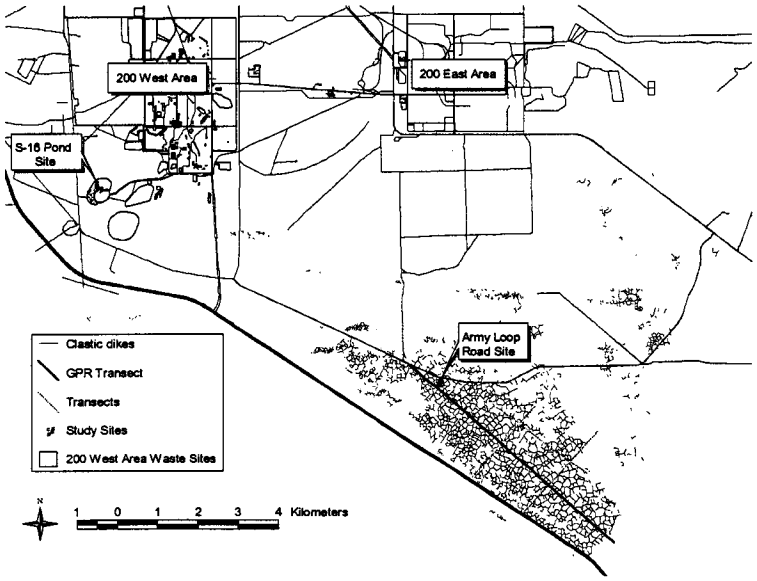

Figure 4. Detailed site map

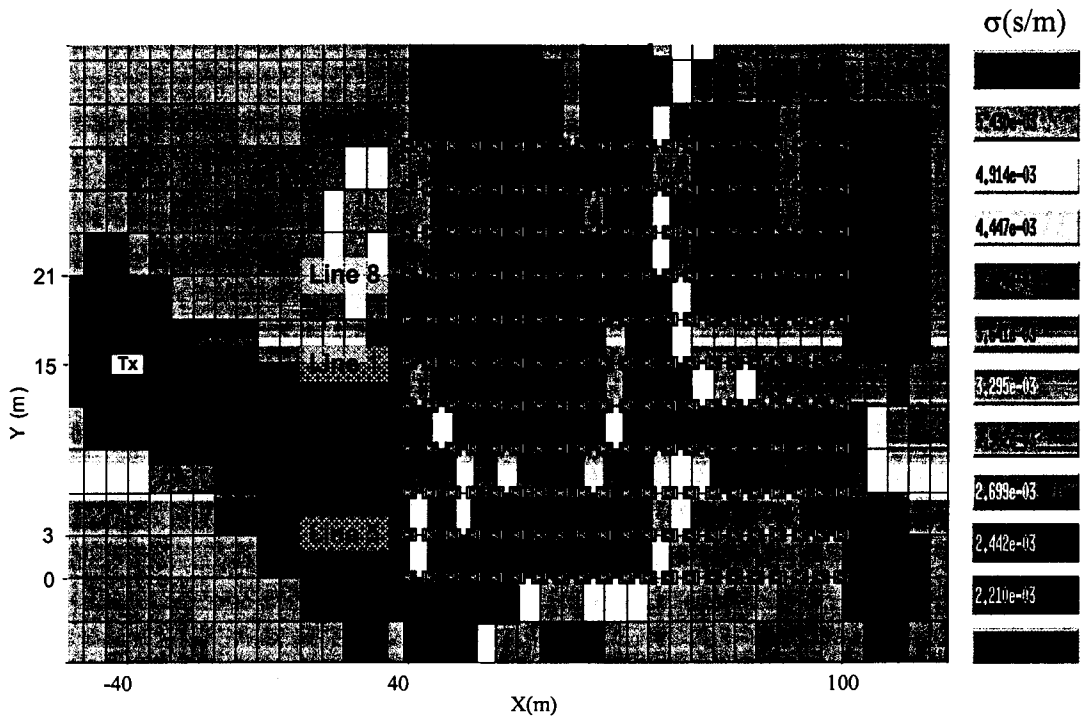

Figure 5. Shown are the transmitter and receiver geometry employed at the Hanford Nuclear Reservation field site. Also shown is the inverted conductivity model at the earth's surface, z=0 m, where the clastic dike structures are indicated in red with a black out

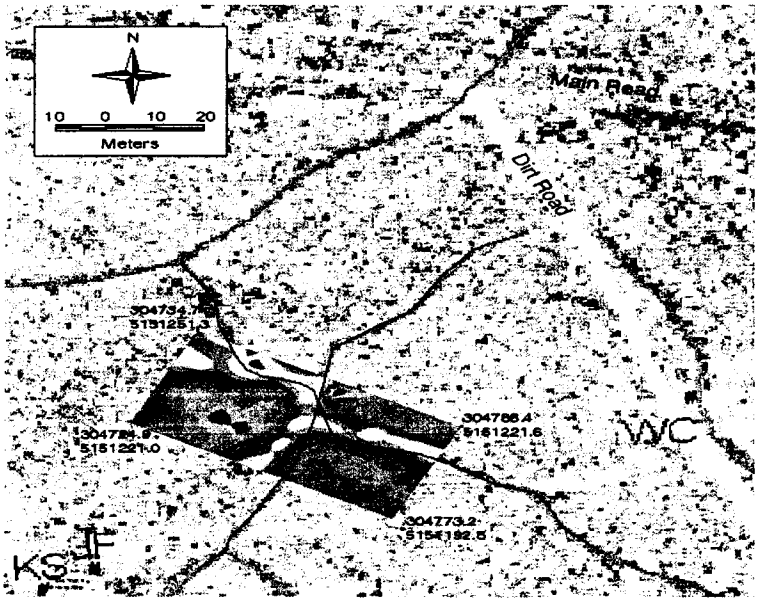

Figure 6. Surface plot of combined impedance data ||(Zxy+Zyx)|| at 66 kHz over the clastic dike site (Army Loop Road Site in Figure 4). The dikes indicated by the yellow to red shading are clearly seen in the plot, and clearly exhibit three-dimensional geometry.

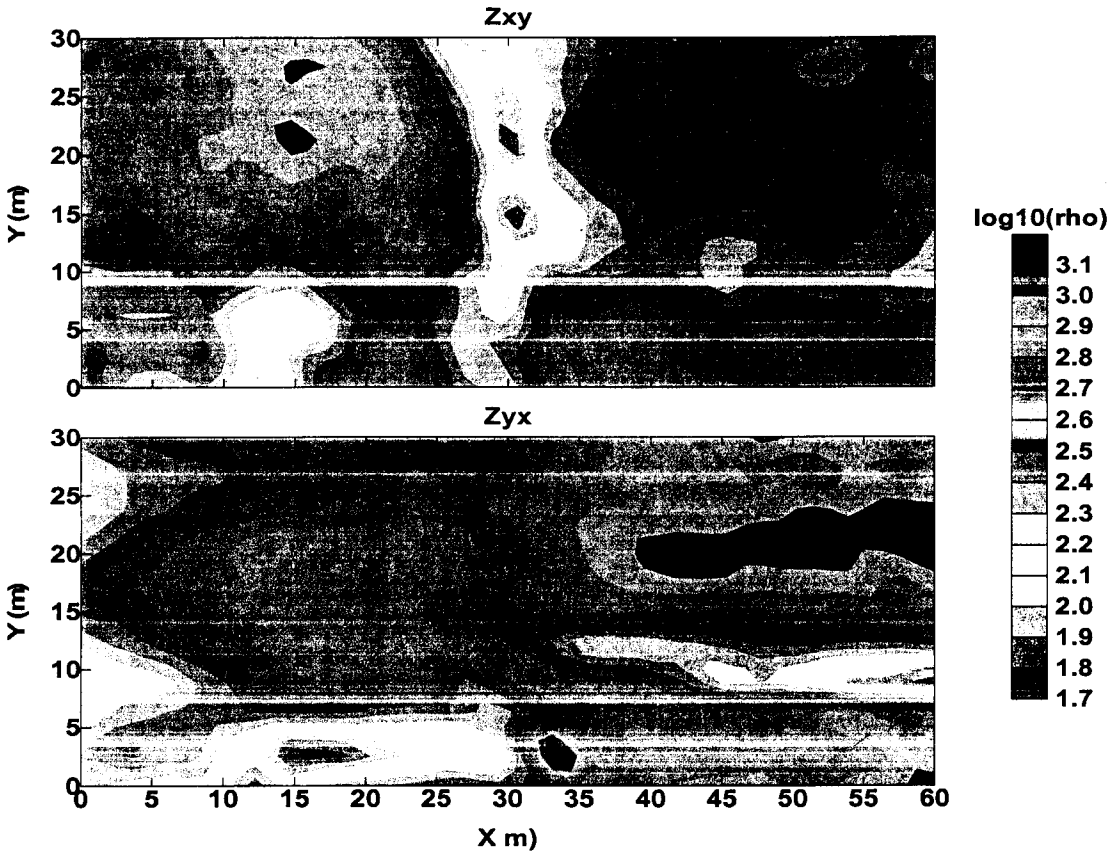

Figure 7. Surface plot of impedance data, Zxy and Zyx, respectively. These data were taken at 66 kHz over the clastic dike site. The dikes indicated by the yellow to red shading are clearly seen in the plot, and clearly exhibit three-dimensional geometry.

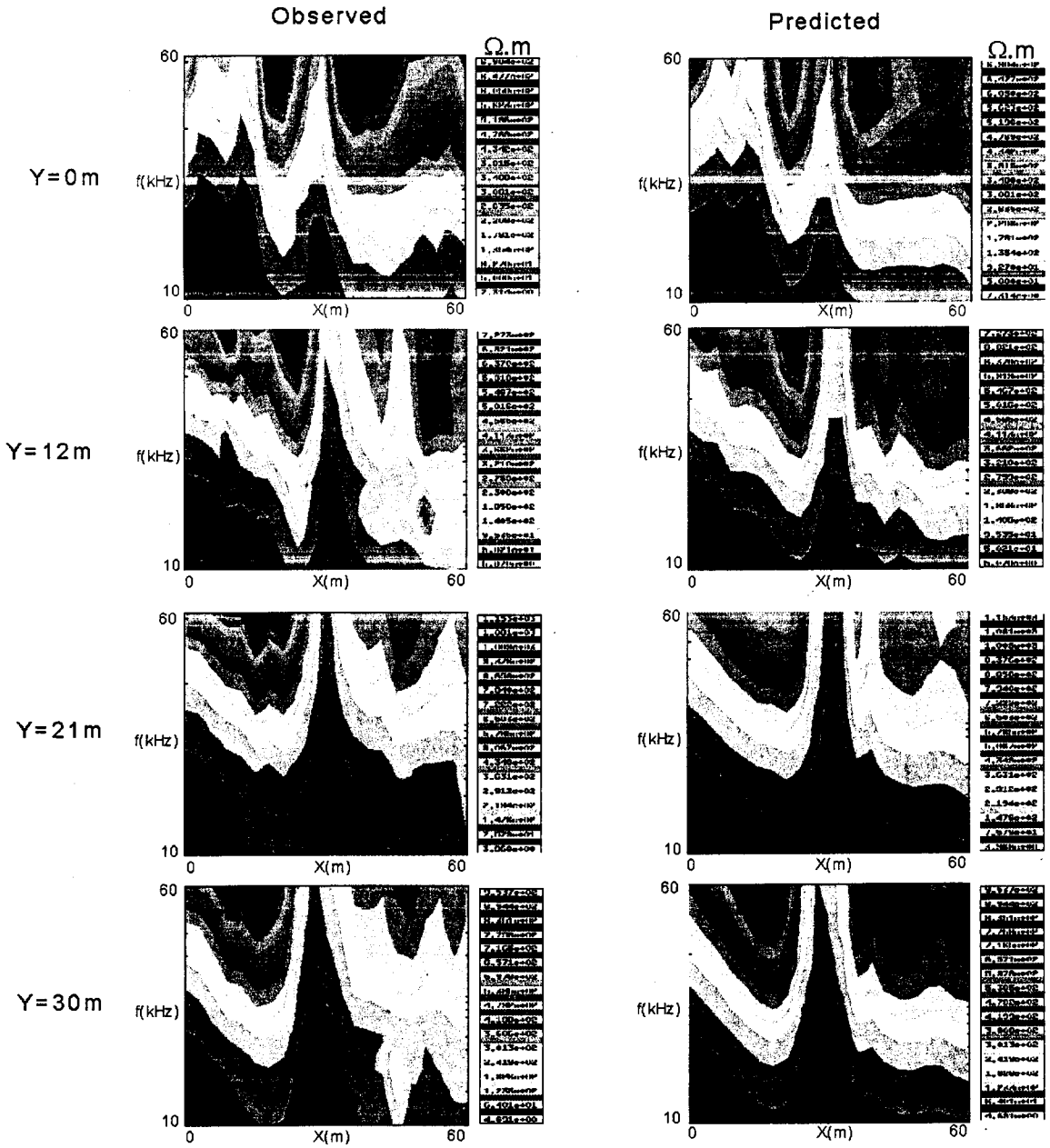

Figure 8. Observed and Predicted Zxy data plotted as apparent resistivity pseudo sections along four profiles in the y coordinate direction.

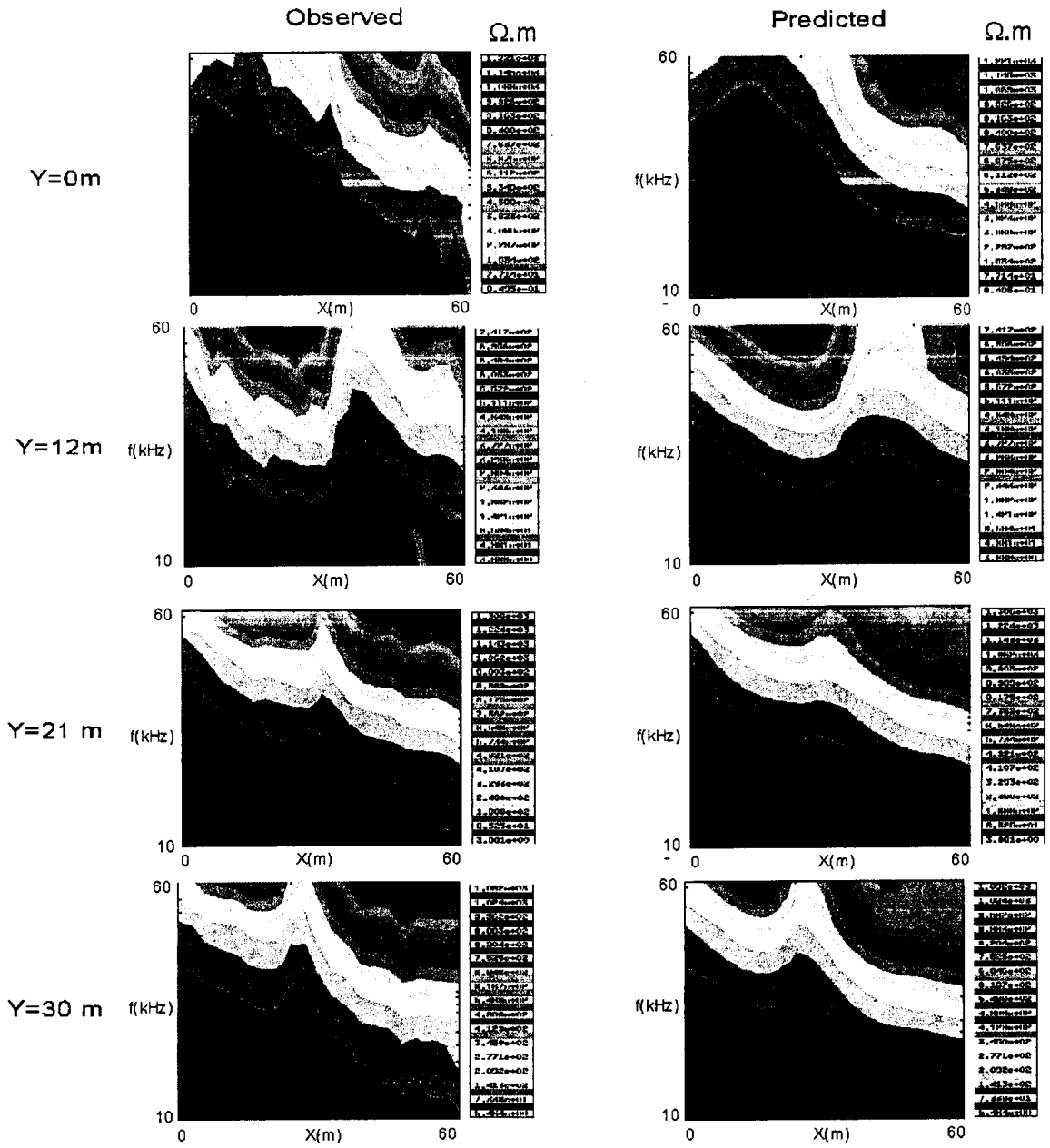

Figure 9. Observed and Predicted Zyx data plotted as apparent resistivity pseudo sections along four profiles in the y coordinate direction.

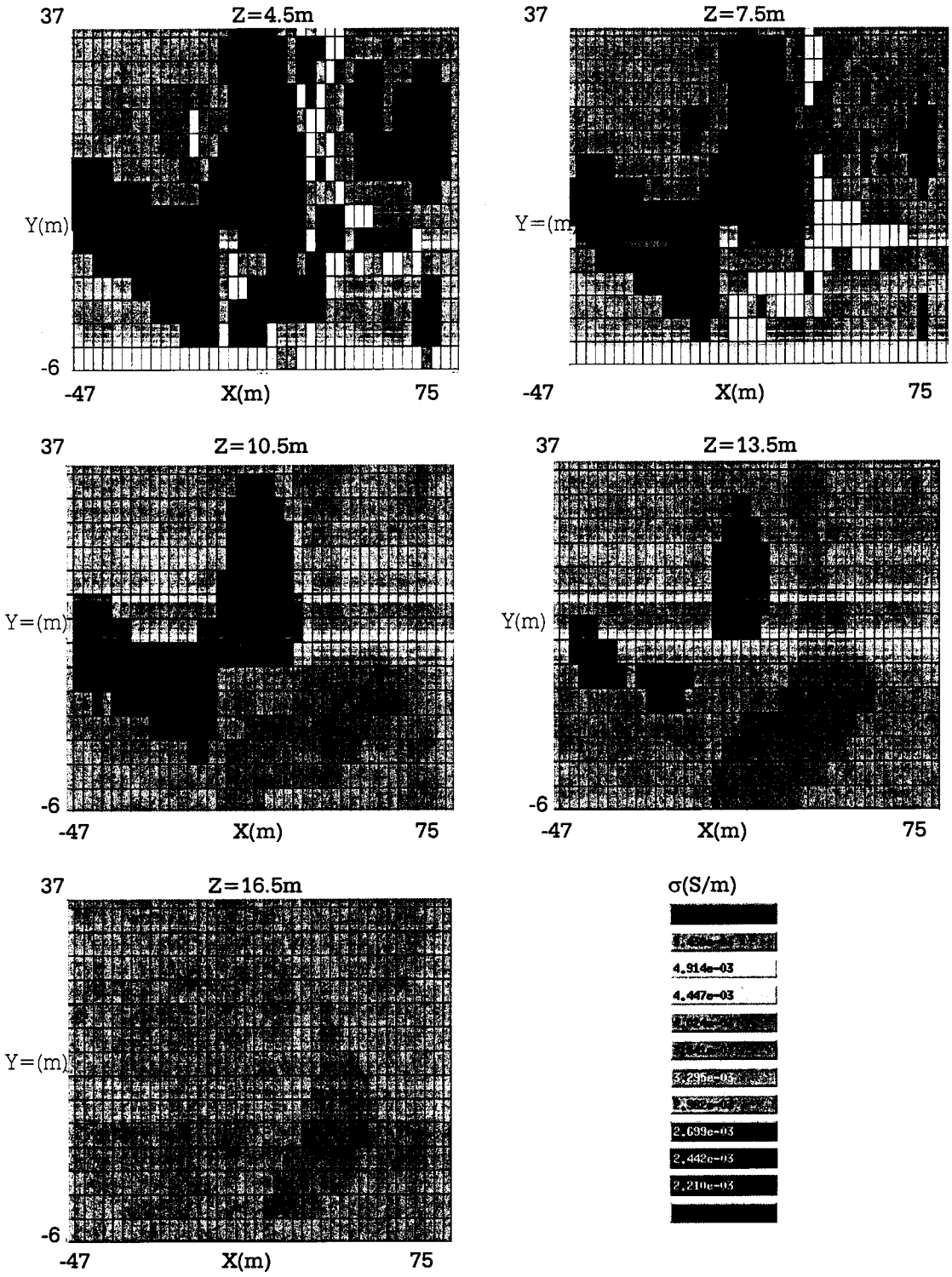

Figure 10. Depth sections of the reconstructed electrical conductivity of the Hanford field data.

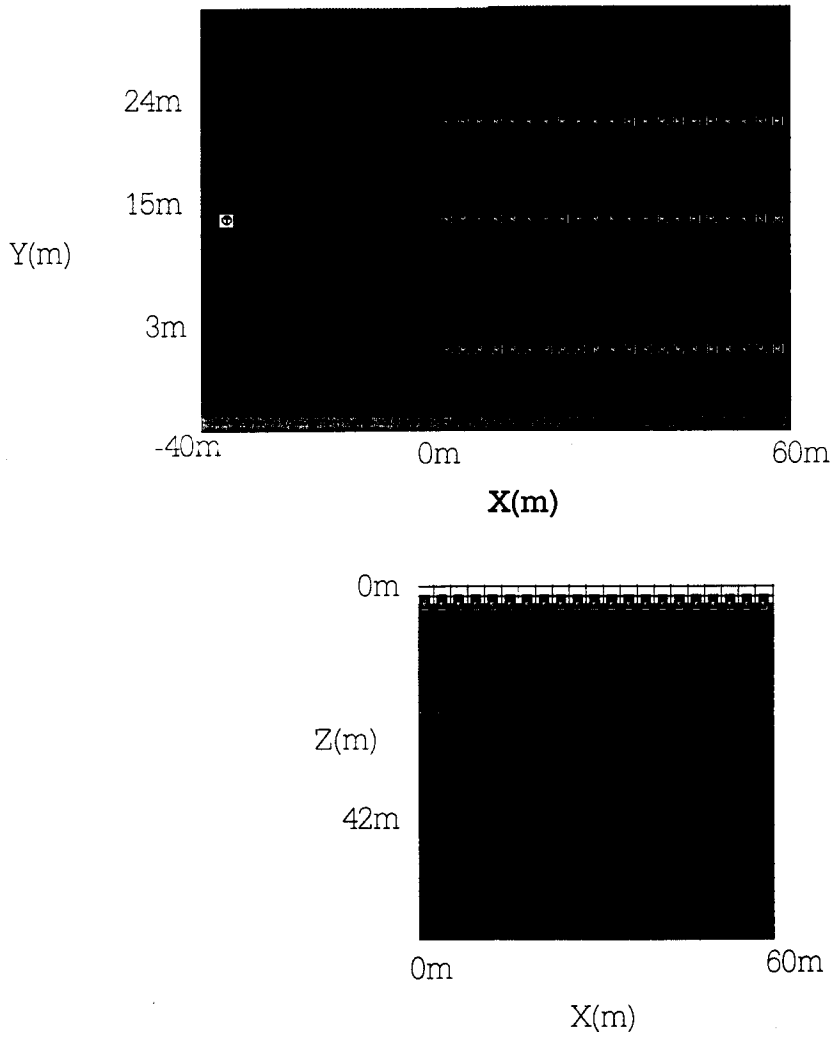

Figure 11. Three-dimensional model used to study the resolving power of near field CSAMT data. Multiple receivers transect the dike, identical to the survey configuration used in the Hanford experiment, but only three of these receiver transects are shown at the

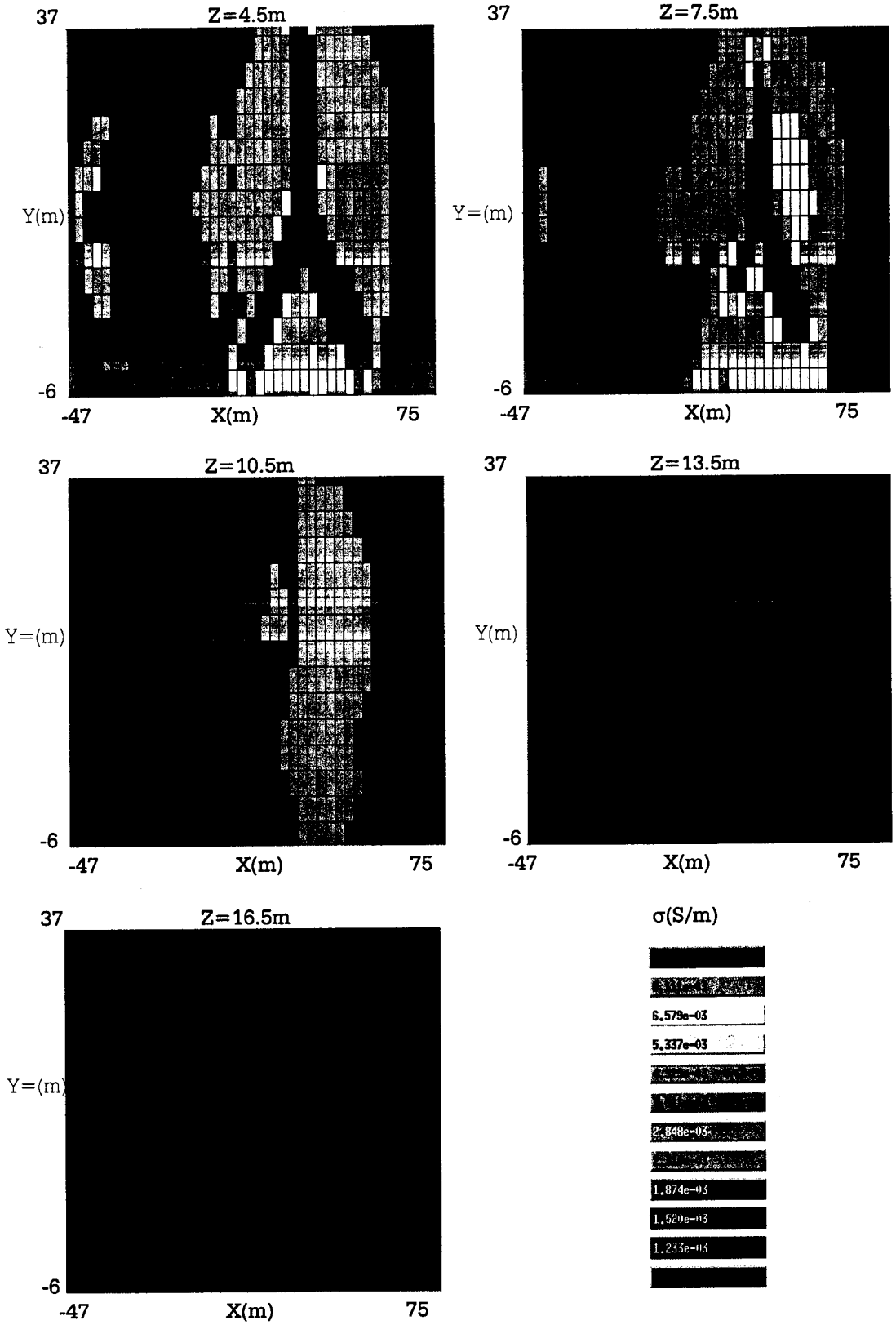

Figure 12. Reconstructed conductivity depth sections for the 3D test model.

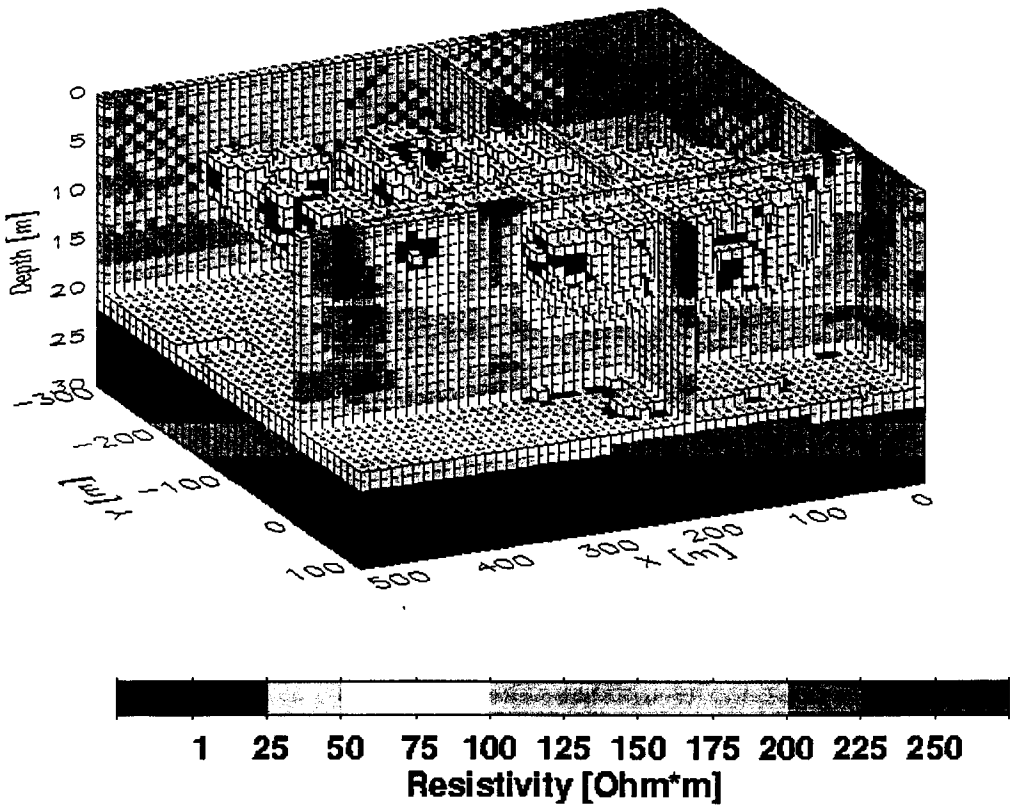

Figure 13. Three-dimensional radio magnetotelluric image of a waste site in Cologne Germany. Resistivities greater than 50 W.m have been rendered invisible, except along selected cross sections. The volumetric extent of the waste is confined to within the top 15